Nonadiabatic Response Model of Laser-Induced Ultrafast π-Electron Rotations in Chiral Aromatic Molecules

Manabu Kanno,[1,*] Hirohiko Kono,[1] Yuichi Fujimura,[1,†] and Sheng H. Lin[2,3]

[1]*Department of Chemistry, Graduate School of Science, Tohoku University, Sendai 980-8578, Japan*
[2]*Institute of Atomic and Molecular Sciences, Academia Sinica, Taipei 10617, Taiwan, Republic of China*
[3]*Department of Applied Chemistry, National Chiao Tung University, Hsinchu 300, Taiwan, Republic of China*

We theoretically investigated the nonadiabatic couplings between optically induced π-electron rotations and molecular vibrations in a chiral aromatic molecule irradiated by a nonhelical, linearly polarized laser pulse. The results of wave packet dynamics simulation show that the vibrational amplitudes strongly depend on the initial rotation direction, clockwise or counterclockwise, which is controlled by the polarization direction of the incident pulse. This suggests that attosecond π-electron rotations can be observed by spectroscopic detection of femtosecond molecular vibrations.

Control of photoinduced electron dynamics of molecules or nanosystems is one of the fascinating research areas in optical, molecular, and nanoscience [1–6]. Investigation of photoinduced electron rotation will provide fundamental clues for designing ultrafast switching devices. For example, in quantum ring systems, quantum dynamical calculations have shown that photoinduced charge currents can be controlled by varying the time delay and strength of the pulses [2]. Optimal control of quantum rings by terahertz laser pulses has been reported as a realistic approach to construct a laser-driven single-gate qubit [3]. In molecular systems, a quantum simulation of π-electron rotation along the aromatic ring of Mg porphyrin with D_{4h} symmetry [4] has been performed [5]. Here, a pair of doubly degenerate excited states, which are complex eigenfunctions of an electronic angular momentum operator, were excited by using a circularly polarized UV laser pulse.

A quantum dynamical simulation of π electrons of an ansa (planar-chiral) aromatic molecule, 2, 5-dichloro$[n](3, 6)$pyrazinophane [DCPH; Fig. 1(a)], has shown that transient rotations of π electrons can be created along its ring by an ultrashort, linearly polarized UV laser pulse [7]. For this molecule, the aromatic ring of C_{2h} symmetry can be fixed to a surface by the ansa group, ethylene bridge $(CH_2)_n$. Doubly degenerate states of D_{6h} benzene are split into two quasidegenerate states in DCPH of C_{2h} ring symmetry. Ultrashort pulses can coherently excite a pair of quasidegenerate states to form a nonstationary state. The relative quantum phase of the initial nonstationary state can be varied by adjusting the spatial configuration of each enantiomer with respect to the polarization direction of the applied pulse. That is, it is possible to construct a nonstationary electronic excited state to rotate π electrons with the initial rotation direction being clockwise or counterclockwise in R and S enantiomers [7]. The rotation direction of π electrons can be con-

trolled by the relative optical phase of a two-color laser as well [8].

Theoretical treatments of photoinduced electron dynamics in previous studies were carried out under a frozen-nuclei condition [5–8], and, to the best of our knowledge, there have been no reports on electron rotation dynamics coupled to molecular vibrations. When π-electron rotation lasts as long as the period of molecular vibrations (several tens of femtoseconds), the electronic and nuclear motions may be coupled to each other. It is well known that nonadiabatic couplings play an essential role in polyatomic molecules even in isolated conditions [9]. Therefore, π-electron rotation should be subjected to undergo nonnegligible nonadiabatic perturbations by nuclear motions. It is important to estimate the effects of nonadabatic couplings in designing ultrafast switching molecular devices. It is also expected that a new method will be found for detecting π-electron rotations by adding vibrational degrees of freedom to an electronic system. In this Letter, we present the results of wave packet (WP) simulations of nonadiabatic dynamics in a model chiral aromatic molecule irradiated by a linearly polarized laser pulse to clarify the effects of π-electron rotation on molecular vibration and vice versa.
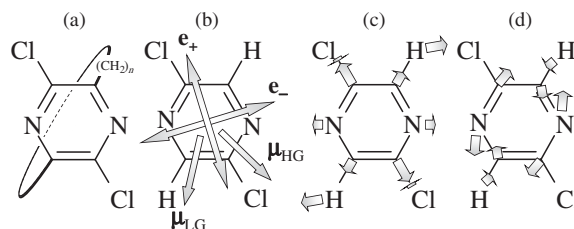
FIG. 1.   Molecular formula of (a) an R enantiomer of DCPH and (b) DCP. The directions of transition moments $\boldsymbol{\mu}_{LG}$ and $\boldsymbol{\mu}_{HG}$ of DCP are shown as well as those of photon polarization vectors $\mathbf{e}_{\pm}$. Vibrational vectors of the (c) breathing and (d) distortion modes of DCP are indicated by thick arrows.

To reduce computational costs, we replaced the ansa group with hydrogen atoms. The simplified model molecule 2,5-dichloropyrazine [DCP; Fig. 1(b)] is not chiral in a strict sense but valid for the investigation of laser-induced π-electron dynamics because π electrons cannot be directly affected by the ansa group with σ electrons.

Ab initio geometry optimization for the ground state of DCP was carried out using MOLPRO [10] at the MP2/6 − $31G^*$ level followed by a single-point ground- and excited-state calculation at the CASSCF(10, 8)/6 − $31G^*$ level. DCP is of C_{2h} symmetry at the optimized geometry of the ground state $|G\rangle \equiv |1^1A_g\rangle$ and has a pair of optically allowed quasidegenerate excited states, $|L\rangle \equiv |3^1B_u\rangle$ and $|H\rangle \equiv |4^1B_u\rangle$, with the energy gap $2\hbar\Delta\omega \equiv 0.44$ eV. The difference between the average energy of the quasidegenerate states and the ground-state energy is 9.62 eV. The directions of the transition electric dipole moments between the quasidegenerate states and $|G\rangle$, denoted as $\boldsymbol{\mu}_{LG}$ and $\boldsymbol{\mu}_{HG}$, and those of the polarization unit vectors $\mathbf{e}_+$ and $\mathbf{e}_-$ defined as $\boldsymbol{\mu}_{LG} \cdot \mathbf{e}_\pm = \pm\boldsymbol{\mu}_{HG} \cdot \mathbf{e}_\pm$, are illustrated in Fig. 1(b).

The effective vibrational degrees of freedom for the WP simulations were determined by performing geometry optimization for $|L\rangle$ and $|H\rangle$ at the CASSCF(10, 8)/6 − $31G^*$ level and it was found that DCP is also of C_{2h} symmetry at the optimized geometry of $|L\rangle$ and that of $|H\rangle$. Hence, vibrational modes with displacements from the optimized geometry of $|G\rangle$ to that of $|L\rangle$ and $|H\rangle$ are totally symmetric modes. Furthermore, vibrational modes that couple two ^1B_u states are also totally symmetric A_g modes. For these reasons, we consider two types of A_g normal modes with large potential displacements and nonadiabatic coupling matrix element, breathing and distortion modes [Figs. 1(c) and 1(d)] whose ground-state harmonic wave numbers are 1160 and 1570 cm^{-1}, respectively. The two-dimensional adiabatic potential energy surfaces (PESs) of $|L\rangle$ and $|H\rangle$ with respect to the breathing and distortion modes were computed at the CASSCF(10, 8)/6 − $31G^*$ level. There exists an avoided crossing between the PESs [11].

The initial nuclear WP was set to be the vibrational ground-state wave function of $|G\rangle$ and then excited by a single-color linearly polarized laser pulse $\boldsymbol{\varepsilon}(t)$. To include the effects of the nonadiabatic coupling on the WP propagation, we expanded the state vector of the system in terms of the three diabatic states $\{|M^D\rangle\}$, constructed as a linear combination of the adiabatic states $|G\rangle$, $|L\rangle$, and $|H\rangle$. The time evolution of the expansion coefficients for $|M^D\rangle$, $\psi_M^D(\mathbf{Q}, t)$, where $\mathbf{Q}$ is the two-dimensional mass-weighted normal coordinate vector, can be obtained from the following coupled equations [12]:

$$i\hbar\partial_t\psi_M^D = -(\hbar^2/2)\nabla^2\psi_M^D$$
$$+ \sum_{M'}[V_{MM'}^D(\mathbf{Q}) - \boldsymbol{\mu}_{MM'}^D(\mathbf{Q}) \cdot \boldsymbol{\varepsilon}(t)]\psi_{M'}^D, \quad (1)$$

where ∇^2 is the Laplacian with respect to $\mathbf{Q}$. $V_{MM'}^D(\mathbf{Q})$ are the diabatic potentials and couplings and $\boldsymbol{\mu}_{MM'}^D(\mathbf{Q})$ are the transition moments between the two diabatic states. The coupled equations were solved numerically with the split-operator method for a multisurface Hamiltonian [13]. The resultant diabatic WPs $\psi_M^D(\mathbf{Q}, t)$ are converted to adiabatic WPs $\psi_M(\mathbf{Q}, t)$.

Figures 2(a) and 2(b) show the temporal behavior in the expectation value of electronic angular momentum $L(t)$ and that of vibrational coordinate $\mathbf{Q}(t)$, respectively, by applying a laser pulse with the linear polarization vector $\mathbf{e}_+$ and that with $\mathbf{e}_-$ (hereafter termed $\mathbf{e}_+$ and $\mathbf{e}_-$ excitations). π electrons with positive (negative) angular momentum travel counterclockwise (clockwise) around the ring in Fig. 1(b). The central wavelength of the pulse was 129 nm corresponding to 9.62 eV of photon energy. To create as much excited-state population as possible, the duration of a sin^2 pulse was set at 7.26 fs and the peak intensities of the pulses with $\mathbf{e}_+$ and $\mathbf{e}_-$ were 5.53 and 9.02 GV m^{-1}, respectively, following the idea of π pulse [14].

In Fig. 2(a), the initial rotation direction of π electrons depends on the photon polarization vector, i.e., clockwise (counterclockwise) direction for $\mathbf{e}_+$ ($\mathbf{e}_-$) excitation, which has been found in a previous paper [7]. The amplitudes of $L(t)$ gradually decay for both cases. The decay of the angular momentum originates from two factors: the decrease of the overlap between the WPs moving on the relevant two adiabatic PESs, which occurs even within
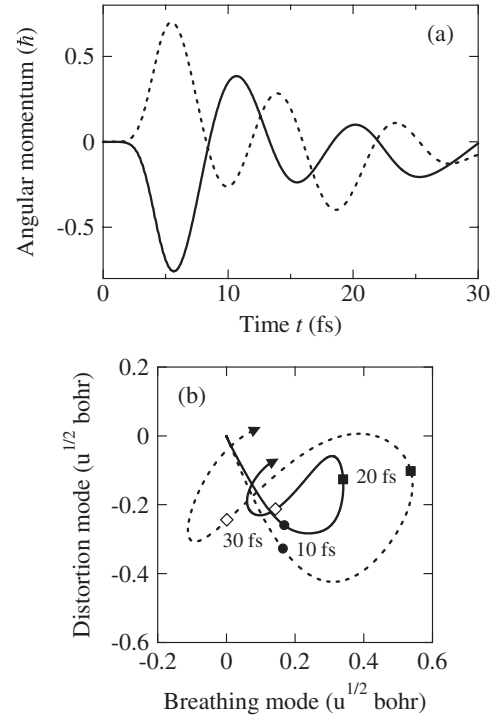
FIG. 2. (a) Expectation value of electronic angular momentum $L(t)$. (b) Expectation value of vibrational coordinate $\mathbf{Q}(t)$. The solid and dotted lines denote the expectation values for $\mathbf{e}_+$ and $\mathbf{e}_-$ excitations, respectively. The values of $\mathbf{Q}(t)$ are plotted up to $t = 40$ fs. The laser pulse ceases at $t = 7.26$ fs.

the Born-Oppenheimer approximation, and the electronic relaxations due to nonadiabatic couplings, which is the major factor. This is one of the characteristic behaviors that are absent in a frozen-nuclei model [5–8]. There are some differences between the oscillatory decays of the angular momentum for $\mathbf{e}_+$ and $\mathbf{e}_-$ excitations. The curve of $L(t)$ for $\mathbf{e}_+$ excitation can be approximately expressed in a sinusoidal exponential decay form with its oscillation period of $\sim \pi/\Delta\omega = 9.4$ fs and lifetime of ~ 7 fs. In contrast, the amplitude of $L(t)$ for $\mathbf{e}_-$ excitation does not undergo a monotonic decrease but makes a small transient recovery around $t \sim 14$–20 fs. Its oscillation period is a little shorter than that for $\mathbf{e}_+$ excitation in this time range. The difference in the oscillation period of the angular momentum for $\mathbf{e}_+$ and $\mathbf{e}_-$ excitations stems from that in the energy gap between the two adiabatic PESs for the regions in which the WPs run. Furthermore, it should be noted that the behaviors of $\mathbf{Q}(t)$ are strongly dependent on the polarization of the applied pulse. The amplitude of $\mathbf{Q}(t)$ for $\mathbf{e}_-$ excitation is more than two-times larger than that for $\mathbf{e}_+$ excitation. This finding is remarkable in the sense that the initial rotation direction of π electrons controlled by the polarization direction of the laser pulse greatly affects the amplitude of subsequent molecular vibration through nonadiabatic couplings. This indicates that molecular chirality can be identified by analyzing vibrational spectra since the rotation direction basically differs between enantiomers according to their alignments with respect to the polarization direction [7].

Temporal behaviors in the population and WP dynamics on the relevant two adiabatic PESs are plotted in Figs. 3(a) and 3(b). For $\mathbf{e}_-$ excitation, the probability densities $|\psi_L(\mathbf{Q}, t)|^2$ and $|\psi_H(\mathbf{Q}, t)|^2$ at $t \sim 5$ fs have almost the same shape as that of the initial WP, while the two excited WPs created are out of phase from the definition of $\mathbf{e}_-$. As the WPs start to move along the gradient of each PES,

significant population transfer occurs from $|H\rangle$ to $|L\rangle$ by nonadiabatic transition. Consequently, the population of $|L\rangle$ at $t \sim 10$ fs is more than 7 times larger than that of $|H\rangle$, although they are almost equal at $t \sim 5$ fs. The loss of a superposition of $|L\rangle$ and $|H\rangle$ reduces the amplitude of $L(t)$ as in Fig. 2(a). Afterwards, the direction of the population transfer is reversed periodically despite the rather small amount of the population transferred; regeneration of the superposition of $|L\rangle$ and $|H\rangle$ around $t \sim 14$–20 fs brings about the transient recovery of the angular momentum. $\psi_L(\mathbf{Q}, t)$ moves in the high-potential region following the potential gradient of $|L\rangle$, which leads to the large-amplitude vibration in Fig. 2(b).

In contrast, $\psi_L(\mathbf{Q}, t)$ and $\psi_H(\mathbf{Q}, t)$ are in phase when DCP is excited by a pulse with $\mathbf{e}_+$. For this excitation, a small amount of the population shifts from $|L\rangle$ to $|H\rangle$ around $t \sim 5$–10 fs. Then, a considerable population transfer takes place in the reverse way around $t \sim 10$–14 fs when the WPs come closer to the avoided crossing. The contours of $|\psi_L(\mathbf{Q}, t)|^2$ at $t = 12.3$ fs in Fig. 3(b) clearly exhibit the node arising from the interference between the WPs. At $t > 14$ fs, the upward population transfer is extremely small. The interference continues to increase (decrease) the probability density in the low-potential (high-potential) region, resulting in the small-amplitude vibration in Fig. 2(b).

The photon polarization dependence of the populations and WPs in Figs. 3(a) and 3(b) can be explained in terms of interferences between the WP existing on the original PES and that created by nonadiabatic couplings. The detailed description of the interference effects will be reported elsewhere.

Finally, we verify that the initial rotation direction of π electrons can be determined by analyzing vibrational spectra. In general, the Fourier transform of the autocorrelation function of WPs gives its frequency spectrum [15]. The
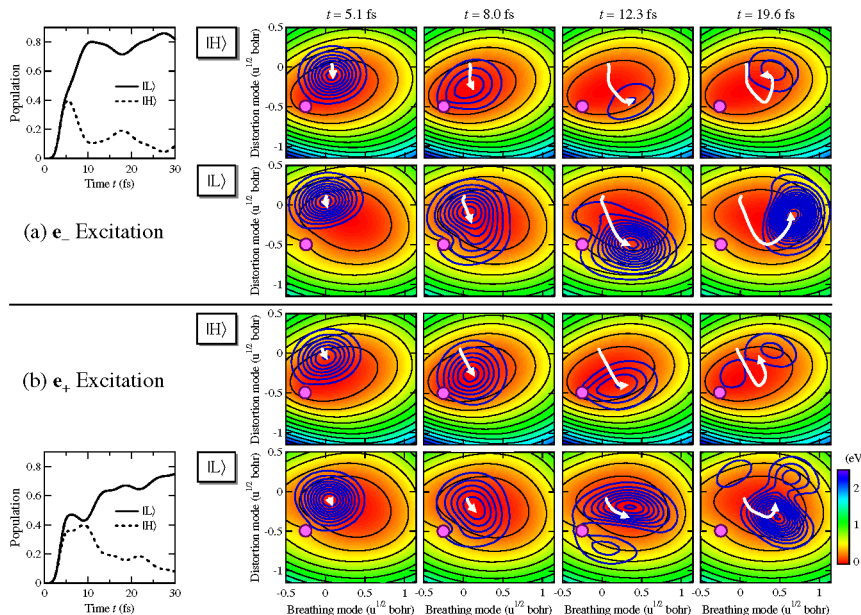
FIG. 3 (color online). Left panel: Temporal behavior in the populations of $|L\rangle$ (solid line) and $|H\rangle$ (dotted line). Right panels: Propagation of the adiabatic WPs on the two-dimensional adiabatic PESs of $|L\rangle$ and $|H\rangle$. The origin of the PESs is the optimized geometry of $|G\rangle$. The bold contours represent the probability densities $|\psi_L(\mathbf{Q}, t)|^2$ and $|\psi_H(\mathbf{Q}, t)|^2$ and the arrows indicate the motion of the center of the WPs. The avoided crossing is signified by a circle.
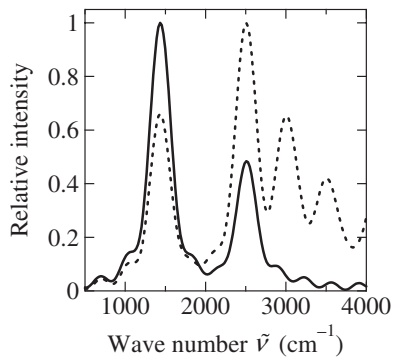
FIG. 4.   The frequency spectra of $\psi_L(\mathbf{Q}, t)$, $\sigma_L(\omega)$, defined in Eq. (2). The solid and dotted lines denote the spectra for $\mathbf{e}_+$ and $\mathbf{e}_-$ excitations, respectively. In each case the values of $\sigma_L(\omega)$ are scaled so that the maximum value is unity.

spectrum of $\psi_L(\mathbf{Q}, t)$ after the nonadiabatic transition from $|H\rangle$ to $|L\rangle$ is defined as

$$\sigma_L(\omega) \equiv \mathrm{Re} \int_{t_i}^{t_f} dt e^{(i\omega - 1/\tau)(t - t_i)} \int d\mathbf{Q}\, \psi_L^*(\mathbf{Q}, t_i)\psi_L(\mathbf{Q}, t).$$

(2)

The parameter τ was introduced to smooth the spectra and set at 39.6 fs, which is longer than the vibrational periods of the breathing and distortion modes (28.8 and 21.2 fs). The values of t_i for $\mathbf{e}_+$ and $\mathbf{e}_-$ excitations were 14.0 and 10.0 fs, respectively, and $t_f - t_i = 99.1$ fs for both cases. The spectra for $\mathbf{e}_+$ and $\mathbf{e}_-$ excitations are displayed in Fig. 4. In the former case, the maximum value of $\sigma_L(\omega)$ appears at $\tilde{\nu} \sim 1400$ cm^{-1} and another peak is found at $\tilde{\nu} \sim 2500$ cm^{-1}; in the latter case, the spectrum reaches its maximum at $\tilde{\nu} \sim 2500$ cm^{-1} and also exhibits a couple of strong peaks at $\tilde{\nu} > 3000$ cm^{-1} [16]. These spectral features confirm that at $t > t_i$ $\psi_L(\mathbf{Q}, t)$ mainly consists of low (high) vibrational quantum states for $\mathbf{e}_+$ ($\mathbf{e}_-$) excitation. The vibrational structure changes of DCP or DCPH can be measured experimentally with optical spectroscopic methods, e.g., transient impulsive Raman spectroscopy [17]. Thus, attosecond π-electron rotations may be observed by spectroscopic detection of femtosecond molecular vibrations that induce nonadiabatic couplings.

In conclusion, we have analyzed the coupling between π-electron rotation and molecular vibration of DCP excited by a linearly polarized UV laser pulse. The angular momentum of π electrons gradually decays, while the vibrational amplitude greatly depends on their rotation direction. The former is attributed mainly to the electronic relaxations caused by nonadiabatic transition; the latter results from the interference in nonadiabatic transition governed by the relative quantum phase between the WPs. From this new insight, the rotation direction of π electrons traveling on an attosecond time scale may be identified by detecting femtosecond molecular vibrations with spectroscopy. Even in the presence of nonadiabatic couplings with a coupling lifetime of ~ 7 fs, π-electron

rotations can produce angular momentum sufficient for ultrafast switching. In this Letter, we have restricted our treatment to DCP. The conclusion above is valid for real chiral aromatic molecules as well.

*Present address: Department of Basic Science, Graduate School of Arts and Sciences, The University of Tokyo, Komaba, 153-8902 Tokyo, Japan.
†fujimurayuichi@mail.tains.tohoku.ac.jp

[1] P. Krause, T. Klamroth, and P. Saalfrank, J. Chem. Phys. **123**, 074105 (2005); M. Nest, F. Remacle, and R. D. Levine, New J. Phys. **10**, 025019 (2008).

[2] A. Matos-Abiague and J. Berakdar, Phys. Rev. Lett. **94**, 166801 (2005).

[3] E. Räsänen, A. Castro, J. Werschnik, A. Rubio, and E. K. U. Gross, Phys. Rev. Lett. **98**, 157404 (2007).

[4] P. Lazzeretti, Prog. Nucl. Magn. Reson. Spectrosc. **36**, 1 (2000); E. Steiner, A. Soncini, and P. W. Fowler, Org. Biomol. Chem. **3**, 4053 (2005).

[5] I. Barth and J. Manz, Angew. Chem. **118**, 3028 (2006); Angew. Chem., Int. Ed. **45**, 2962 (2006); I. Barth, J. Manz, Y. Shigeta, and K. Yagi, J. Am. Chem. Soc. **128**, 7043 (2006).

[6] K. Nobusada and K. Yabana, Phys. Rev. A **75**, 032518 (2007).

[7] M. Kanno, H. Kono, and Y. Fujimura, Angew. Chem. **118**, 8163 (2006); Angew. Chem., Int. Ed. **45**, 7995 (2006).

[8] M. Kanno, K. Hoki, H. Kono, and Y. Fujimura, J. Chem. Phys. **127**, 204314 (2007).

[9] S. H. Lin, J. Chem. Phys. **44**, 3759 (1966); M. Bixon and J. Jortner, *ibid.* **48**, 715 (1968).

[10] H.-J. Werner *et al.*, MOLPRO, version 2006.1 (Cardiff, UK, 2006).

[11] We confirmed by a CASPT2 calculation that the avoided crossing remains unchanged when dynamical electron correlation is taken into account, while the PESs are lowered by ~ 3 eV.

[12] Y. Ohtsuki, K. Nakagami, and Y. Fujimura, in *Advances in Multi-Photon Processes and Spectroscopy*, edited by S. H. Lin, A. A. Villaeys, and Y. Fujimura (World Scientific, Singapore, 2001), Vol. 13, p. 1.

[13] P. Gross, D. Neuhauser, and H. Rabitz, J. Chem. Phys. **96**, 2834 (1992).

[14] B. W. Shore, *The Theory of Coherent Atomic Excitation* (Wiley, New York, 1990), Vol. 1, pp. 304–309.

[15] D. J. Tannor, *Introduction to Quantum Mechanics: A Time-Dependent Perspective* (University Science Books, California, 2007), p. 81.

[16] The wave numbers of 1400, 2500, and 3000 cm^{-1} are very close to those of the lowest three vibrational states of $|G\rangle$ owing to the similarity between $|G\rangle$ and $|L\rangle$ in the PES around its minimum.

[17] S. Takeuchi, S. Ruhman, T. Tsuneda, M. Chiba, T. Taketsugu, and T. Tahara, Science **322**, 1073 (2008).